Damage tolerance in ductile woven silk fibre thermoplastic composites

Alexandros Prapavesis [1], Penelope Kopana [1], Weijing Wu [2], Jeroen Soete [1], Yasmine Mosleh [3], Aart Willem van Vuure [1]

[1] Department of Materials Engineering, KU Leuven, Heverlee, Belgium (alexandros.prapavesis@kuleuven.be)

[2] College of Energy and Power Engineering, Nanjing University of Aeronautics and Astronautics, Nanjing, China

[3] Biobased Structures and Materials Group, Department of Engineering Structures, Faculty of Civil Engineering and Geosciences, Delft University of Technology, the Netherlands

In this study, the tensile and bending properties of silk fibre composites using three (0, 90) woven fabrics with different architectures are investigated. The tensile results show that the silk composites can achieve high strain to failure (more than 20%) and toughness (up to 13 MJ/m^3), which can be further manipulated based on the architecture of the fabrics, thus providing more tailored properties and design freedom in applications. XCT and SEM characterization are used to investigate and explain the outstanding toughness of these composites. In tension, a high density of microcracking was observed away from the failed location, which could explain the intrinsic high ductility and energy absorption of silk fibre composites by means of damage spreading throughout its volume in contrast to inherently brittle materials. In bending, significantly lower properties were observed with the more striking being the strain at failure reaching only 30% of the tensile value, thus limiting the potential of silk fibres in bending-dominated loading configurations. XCT revealed that the lower performance is due to failure on the compressive side of the composites, where a clear characteristic kink-band was observed in all composites subjected to bending, while there was no visible damage on the side under tension. This behaviour is also linked to the soft HDPE polymer matrix used, which provides little resistance to fibre buckling.

Keywords: Biocomposite, ductility, damage tolerance, X-ray computed tomography

1 Introduction

In the last two decades, natural fibres as reinforcement in polymer matrix composites have attracted a lot of attention in the composites industry due to their, compared to traditional materials, outstanding specific mechanical properties coupled with advantages such as environmentally friendly and renewable nature, which they owe to their bio-based character. Furthermore, natural fibres have a low energy demand during production, are (potentially) low-cost and have additional interesting physical properties like remarkably good vibrational damping and a low coefficient of thermal expansion [1, 2]. However, the most commonly used natural fibres, which often are plant-based such as flax, hemp, bamboo and jute, typically have restricted use in impact sensitive applications due to their low strain to failure range falling between 1% to 3% [3–5] resulting in a brittle nature and thus low toughness and poor impact performance [6–8]. On the other hand, the use of the (animal protein) natural silk fibre towards structural applications has shown considerable growth in the research community due to a better combination of high (absolute and specific) strength, moderate modulus and outstanding toughness. Toughness values found for silk include these from *Bombyx mori* silkworm produced silk (70 MJ/m^3), spider produced silks *A. diademantus* MA (160 MJ/m^3) and *Nephila edulis* Dragline (215 MJ/m^3) which means silk fibres outperform even traditional highly ductile synthetic fibres like Kevlar 49 (50 MJ/m^3) [9, 10]. Additionally, in contrast to plant-based fibres, silk fibres exist in continuous filaments typically with a length above 1 km, thus allowing the production of continuous fabrics for composite applications. It is worth mentioning that, as presented in Table 1, spider silk can outperform silk produced by silkworms essentially in any mechanical aspect with fibre properties designed and evolved by nature for about 300-400 million years [11, 12] to even stop flying insects with high kinetic energy, hence it is often described as a "super-fibre" [9, 13]. However, mass production of spider silk, particularly in volumes required for structural applications, is at this moment not feasible due to the cannibalistic nature of spiders to maintain control of their local population dynamics [14]. Research is conducted to overcome this mass production problem by genetic incorporation of the native spider silk genes responsible for the production of their silk proteins to *Bombyx mori* silkworms and use them as natural spinners, achieving interesting results [15, 16], but the technology is still under development. Therefore, hereafter any mention of silk will refer to conventional silkworm-produced fibres.

According to the silk fibres' aforementioned properties, summarized in Table 1, it can be identified that there is a high potential for commercial use of silk fibre-reinforced composites in impact sensitive applications (e.g., silk/HDPE protective helmets [17]) or as a supportive element to improve the toughness in impact-critical strategic locations of a structure, possibly via fibre hybridization [18], particularly in areas where barely visible impact damage can occur and propagate rapidly to sudden catastrophic failure.

Table 1. Commonly investigated silk fibre mechanical properties compared to traditional ductile synthetic fibres. Data collected from the review works of [10, 19, 20] and research works of [13, 21–26].

Fibrous material	Density (g/cm^3)	Strength (GPa)	Stiffness (GPa)	Strain at failure (%)	Toughness (MJ/m^3)
B. mori silkworm silk	1.3	0.6	16	18	70
A. diademantus MA spider silk	1.3	1.1	10	27	160
A. diademantus Flag spider silk	1.3	0.5	0.003	270	150
Nephila edulis Dragline spider silk	1.3	1.1	8-13	39	215
Nephila clavipes Dragline spider silk	1.3	0.7 - 1.7	19.5 - 35	6 - 12	-
Nylon	1.1	0.95	5	18	80
Kevlar 49	1.4	3.6	130	2.7	50
Steel	7.8	0.67	193	19.5	52*

*Toughness was back-calculated from the stress-strain curve with data provided by the authors of [26].

Generally, the matrix of the composite plays a crucial role since it determines the level of base adhesion with the silk fibres, and the selected matrix, as observed by van Vuure et al. [27], can often determine the strain to failure of the composite. The fracturing of a brittle thermoset polymer matrix, with a far lower strain to failure compared to the silk fibres, will lead to complete composite failure, thus not allowing the silk fibres to reach their full potential. This is further supported in the bibliographic data presented in Table 2, where significantly lower strain at failure for thermoset matrix composites is often observed compared to their thermoplastic matrix counterparts [27–31]. On the other hand, although the resulting ductility of the composite is remarkably lower, the flexural strength of epoxy matrix composites is superior to this for thermoplastic composites, hypothesized due to the

absence of damage development in the compressive region of the composites since thermoset matrices are often characterized by high stiffness, providing more support to the fibre against compressive loads and preventing fibre kinking [32].

Another notable remark is the lower tensile to flexural strength ratio of the silk-epoxy composites, which is explained by the difference in defect sensitivity of each test. Since in tension the whole material volume is loaded under the maximum stress, the critical defects are also loaded in this condition, which in brittle materials can often determine the failure. In bending, only the mid-point is experiencing the maximum stress, which makes this loading condition less sensitive to the presence of defects. In contrast, the thermoplastic matrix composites are more ductile and thus are less sensitive to defects, as well as usually having higher strain to failure than the silk fibres, hence delaying the tensile failure, but with the disadvantage of weaker performance in bending, which is deteriorating as an inverse function of the stiffness of the matrix due to the weaker support to the fibres against compressive loads.

Due to their inherent complex inhomogeneous and anisotropic microstructure, the toughness and fracture of composites is rarely a simple case because of the presence of various energy absorption mechanisms, which contribute with different intensity in the total energy dissipation capability of the material. Matrix cracks, fibre failure, delamination, fibre pull-out and debonding are the main controlling mechanisms, depending on the type of the fibre and matrix materials, but also depending on the base fibre/matrix adhesion [37–39]. For the latter, it is well known that, as the level of base adhesion decreases, the work of fracture increases until a certain limit [37] by activating a larger contribution of the strong energy absorption mechanisms of debonding and fibre pull-out. Yang et al. [40] compare the toughening mechanisms of silk composites in combination with three typical epoxy systems with different levels of adhesion (weak to strong) and different levels of strain at failure ($\varepsilon_{failure}$) from brittle with $\varepsilon_{failure}$<3% to ductile with $\varepsilon_{failure}$ >60%, larger than the failure strain of the fibres. The authors report for the ductile epoxy composite system fracture mechanisms associated with the inherent toughness of the fibres, while for the more brittle epoxy systems, microcracking and crack deflection were observed as the dominant toughening mechanisms.

In [27], fractography observations revealed that the matrix selection, and by extension the fibre/matrix interface, plays a crucial role in the failure mechanisms, as the strongly

Table 2. Bibliographic review of silk fibre reinforced composites' tensile and flexural properties with different matrices

Type of composite	Volume fraction (%)	Tensile mechanical properties			Flexural mechanical properties			Tower drop impact	Ref.
		Stiffness (GPa)	UTS (MPa)	Strain at failure (%)	Stiffness (GPa)	UFS (MPa)	Strain at max stress (%)	Energy absorption (J/mm)	
Nonwoven Silk-Epoxy	36.2	5.4 ± 0.2	60 ± 5	1.3 ± 0.2	5.2 ± 0.2	143 ± 0.2	3.4 ± 0.4	-	[28]
Plain woven Silk-Epoxy	45.2	6.5 ± 0.1	111 ± 2	5.2 ± 0.2	6.4 ± 0.4	250 ± 4	6.9 ± 0.2	-	[28]
Plain woven Silk-Epoxy	59.12	7.4 ± 0.1	153.5 ± 3.7	4.5 ± 0.1	10.5 ± 0.1	343.8 ± 5.1	4.5 ± 0.1	-	[29]
Plain woven Silk-Epoxy	69.59	7.8 ± 0.2	176.9 ± 2.6	4.8 ± 0.1	12.5 ± 0.1	265.7 ± 9.0	3.8 ± 0.0	-	[29]
Random Mat Silk-Epoxy	30	-	-	-	4.5 ± 0.27	150 ± 4.1	5.7 ± 0.6	-	[30]
Plain weave Silk-Epoxy	30	-	-	-	5.4 ± 0.2	164.5 ± 3.1	5.3 ± 0.2	-	[30]
Unidirectional Silk-Epoxy	-	5.89 ± 0.39	127.8 ± 1.48	14.10 ± 0.5	5.97 ± 0.11	193.76 ± 4.66	-	-	[31]
Twill weave Silk-Epoxy	40	6.2 ± 0.3	115 ± 7	4.1 ± 0.6	-	-	-	2 ± 0.5	[27], [33]
Twill weave Silk-CoPP	49	4.2 ± 0.1	133 ± 2	11.7 ± 0.5	3.6 ± 0.5	67 ± 0.5	1.76 ± 0.02	25.5 ± 0.5	[27], [33]
Twill weave Silk-PPgMA	46	4.8 ± 0.6	140 ± 1	11.2 ± 0.4	4.5 ± 0.05	114 ± 2	2.12 ± 0.03	15.5 ± 0.5	[27], [33]
Twill weave Silk-PBS	51	4.3 ± 01	134 ± 2	11.4 ± 0.5	4.4 ± 0.1	68 ± 4	1.51 ± 0.04	23.0 ± 2.5	[27], [33]
Twill weave Silk-PBSa	52	4.2 ± 0.4	130 ± 3	11.6 ± 0.9	-	-	-	38.5 ± 3	[27], [33]
Unidirectional Silk-PP	15	0.79 ± 0.03	55.1 ± 0.8	-	3.45 ± 0.2	56.3 ± 1	-	-	[34]
Unidirectional Silk-Fibroin	10	3.1 ± 0.2	83 ± 7	11.2 ± 1.3	-	-	-	-	[35]
Unidirectional Silk-Fibroin	20	3.0 ± 0.2	142 ± 7	23.5 ± 1.7	-	-	-	-	[35]
Unidirectional Silk-Fibroin	25	2.8 ± 0.1	151 ± 5	27.1 ± 1.4	-	-	-	-	[35]
Injection mould Silk-PLA	5	4.08 ± 0.05	70.6 ± 1.1	3.8 ± 0.5	4.06 ± 0.2	97.41 ± 21.8	2.9 ± 0.99	-	[36]

bonded epoxy and PP-g-MA-matrix composites displayed flat fracture surface topography for both fibres and matrix, while the CoPP-matrix composites were characterized by long clean fibres without any matrix residue, indicating extensive debonding and fibre-pull out. For the elastomeric PBS-matrix composite, the fracture topography revealed an adhesion failure in between that of CoPP and PP-g-MA with fibre pull-outs still visible but with shorter fibre lengths being pulled from the matrix. The toughness mechanism response against impact loads (Charpy impact [41] and tower drop impact [42]) consisted of a combination of matrix cracking, fibre fracture, delamination, debonding and pull-out, which explains the exceptional resistance of silk fibre reinforced composites in that type of loading scenario.

It is worth mentioning that all aforementioned studies identified the failure mechanisms visually after testing with scanning electron microscopy (SEM) fractography analysis. Tian et al. [43], studied the sequence and contribution of damage mechanisms of silk-epoxy composites and their constituents before and after exposure to humid environments using the acoustic emission (AE) method. The main AE signals showed, that for the dry composites, matrix cracks and debonding dominated the failure and for the highly wet composites the presence of debonding was even more present due to the plasticization effect of water on the fibres and the interfacial degradation caused by the absorbed water.

In this study, silk produced from *Bombyx mori* in the form of woven textiles with different architectures is studied, having different levels of anisotropy by varying warp and weft fibre ratios and by use of straight or twisted fibres. These fabrics were used to produce composites in combination with a highly ductile thermoplastic matrix. First, a thermal analysis of the silk fibre and the matrix was conducted to evaluate the processing temperature, since it is known that the fibres can thermally degrade at elevated temperatures [44, 45], accompanied by a colour transition from white to yellow. The resulting mechanical properties of the produced composites were evaluated in tension and bending, and the failure mechanisms were investigated using SEM surface fractography together with non-destructive 3D X-ray computed tomography (XCT). While the image resolution of SEM, a surface imaging technique, is typically higher than for an industrial XCT, the latter allows the internal investigation of the volume in 3D, without the need to cut, polish, or coat the material. XCT imaging was also used for quality control of the manufactured composites towards, amongst others, the presence of manufacturing defects.

2 Materials and methods

*2.1 **Materials***

Bombyx mori silk woven fabrics (0,90) with different fabric architectures were provided by Sport Soie (France). The areal density and architecture description of each fabric direction is given in Table 3. The silk weaves were degummed by the supplier before they were used as reinforcement in this research. As matrix material, the thermoplastic polymer high-density polyethylene grafted with maleic anhydride (HDPE-g-MA), under the tradename Bynel® 40E529, was selected for its high ductility (>500% strain to failure) while maintaining relatively good adhesion with the silk fibres due to the maleic anhydride grafting [27]. This matrix was kindly provided by DuPont, Belgium and extruded to thin films of 65 µm thickness by Amcor Flexible, Belgium.

Table 3. Areal density and fibre volume isotropy of warp and weft directions of the used silk fabrics

	Warp direction (g/m^2)	Weft direction (g/m^2)	Warp/weft fibre areal density ratio isotropy (%)	Fabric architecture in warp & weft directions
F1 fabric	43.5	43.5	100.0	Warp & weft with no twists
F2 fabric	47.0	42.0	111.9	Warp with no twists & weft with twisted fibres
F3 fabric	96.4	79.6	121.1	Warp with no twists & weft with twisted fibres

*2.2 **Composite production***

The composites were manufactured using the film stacking compression moulding method, where polymer films of the matrix are stacked alternately between the fabrics inside a stainless-steel frame. The frame is used to control the final dimensions of the laminate, hence providing good control over the theoretically calculated fibre volume fraction V_f and preventing overflow of the molten polymer outside of the laminate when high pressure is applied. In this study, for all composites, a V_f of 40% was targeted. The laminate was placed in a pre-heated hydraulic hot-press (Fontijne, Belgium) and compressed under 15 bars and a temperature of 145 ^oC for 10 min, followed by a cooling down step, using the internal water-cooling system (approximately 30 ^oC/min cooling

speed) of the hot-press. The pressure is maintained during the cool down to room temperature. The reasoning behind the used processing temperature is explained in result section 3.2.

2.3 Thermal analysis

2.4 Differential scanning calorimetry (DSC)

DSC measurements were carried out to characterize the thermoplastic matrix using a T.A. Instruments Q2000 calorimeter. The tests were performed with a nitrogen flow of 50 mL/min and a heating rate of 10 °C/min for a temperature range of 30-200 °C.

2.5 Thermogravimetric analysis (TGA)

Isothermal TGA measurements were performed on the pure fibres at 145°C, 155°C and 165°C for 1 hour, to observe any potential thermal degradation of the fibres which could occur during the manufacturing of the composites. Because of the hydrophilic nature of the silk, the fibres were pre-dried for 1h at 90°C.

2.6 Mechanical characterization

2.7 Tensile testing

The tensile properties were tested in accordance with the ASTM D3039 standard using an INSTRON 5567 apparatus equipped with a 30 kN load cell and an extensometer to measure the strain with higher precision.

2.8 Flexural testing

The 3-point bending flexural properties were characterized following the ASTM D790M standard using the same INSTRON 5567 apparatus but in combination with a 1 kN load cell. The strain was calculated using the measured crosshead displacement; since the forces developed during the flexural testing were in the range of ~100 N (in contrast to the kN-scale forces developed in tension) the machine compliance was considered negligible.

2.9 X-ray computed tomography (XCT)

XCT scanning of the tensile and flexural specimens was performed at the KU Leuven XCT Core Facility, on a TESCAN UniTOM HR, equipped with a 160 kV/25 W X-ray tube, with a tungsten transmission target and a 16-bit detector of 2916 × 2280 pixels, and a 50 µm pixel

pitch. The scans were performed at 60 kV and 4 W, using the high-power focus mode, accompanied by a voxel size of 4 µm. In total 3000 radiographic projections were collected over a 360° sample rotation, each with an exposure time of 240 ms and frame averaging set to 5.

For all acquired scans, the radiographic projections were reconstructed to cross-sectional tomographic slices using a filter back-projection algorithm in the TESCAN reconstruction software Panthera. All post-processing and data visualization was performed in Avizo 3D v2022.1 (ThermoFisher).

2.10 Scanning electron microscopy (SEM)

The fabrics and failed composites were inspected at different magnifications up to x8000 using a Philips XL30 Field Emission Gun (FEG) SEM to investigate the fibre architecture and the resulting failure behaviour in both warp and weft directions of the fabric. The acceleration voltage and spot size were 30 kV and 3 nm respectively. Prior to the SEM inspection, all specimens were pre-dried and sputter-coated with a 5nm Pd/Pt coating.

3 Results

3.1 Thermal analysis of the composite manufacturing conditions

The thermal properties of the matrix and silk fibres were investigated to determine the processing parameters that would allow the manufacturing of a composite without degrading or changing the colour of the thermally sensitive fibres. Figure 1a shows the DSC thermograms of the polymer matrix where its melting point can be identified at 133.6 °C, while the melting of the last crystal occurs at 140.3 °C. Additionally, Figure 1b presents the thermal degradation analysis of the silk fibres used in this study. The initial weight drop, during the ramp-up to the drying temperature, is related to the loss of water that was absorbed by the fibres. Then, the weight was stable for 1h, meaning that all water had been removed from the specimens. Following the drying step, the temperature was increased to perform the iso-thermal TGA. For all three selected temperatures 145°C, 155 °C, and 165 °C, a small weight drop was detected. Motta et al. [45] observed a similar small weight drop in the same temperature range after the drying step, which was attributed to the evaporation of other low-temperature volatile substances. Thereafter, the fibres remained essentially stable at all temperatures, with a weight drop of < 0.1% for the 10 min composite processing time and < 0.3% drop after 1h (Figure 2), even for the highest

selected temperature of 165 °C. Therefore, it is concluded that the selected composite manufacturing time and temperature were sufficient to melt the matrix without affecting the fibre integrity.

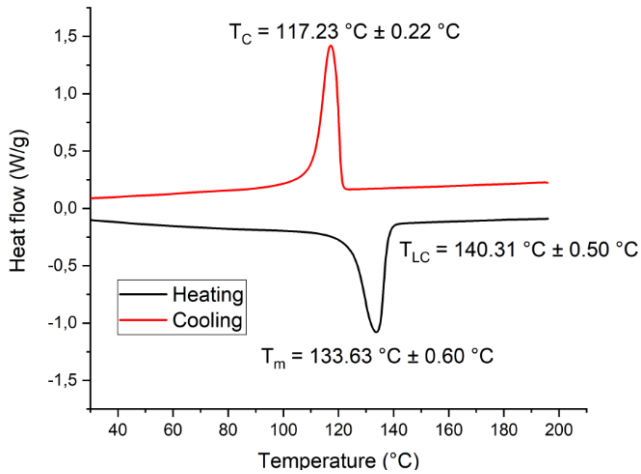

Figure 1a. DSC heating-cooling cycle of the matrix polymer HDPE-MA and

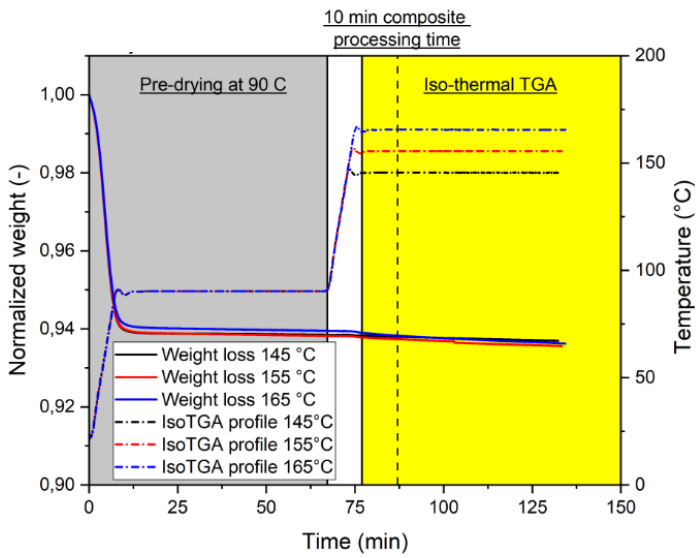

Figure 1b. isothermal TGA thermal degradation of silk fibres

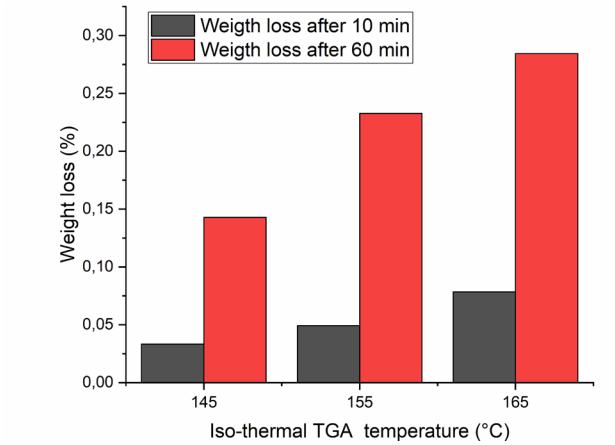

Figure 2. Weight loss during the iso-thermal TGA step after 10 min and 60 min

Additionally, in Figure 3 the impregnation quality after manufacturing of the composites can be qualitatively evaluated using SEM imaging. It is observed that the matrix has penetrated in between the individual fibres inside the silk fibre yarns, thus resulting in good wetting and impregnation, further supporting the selected manufacturing parameters and thus the quality of the produced composites.

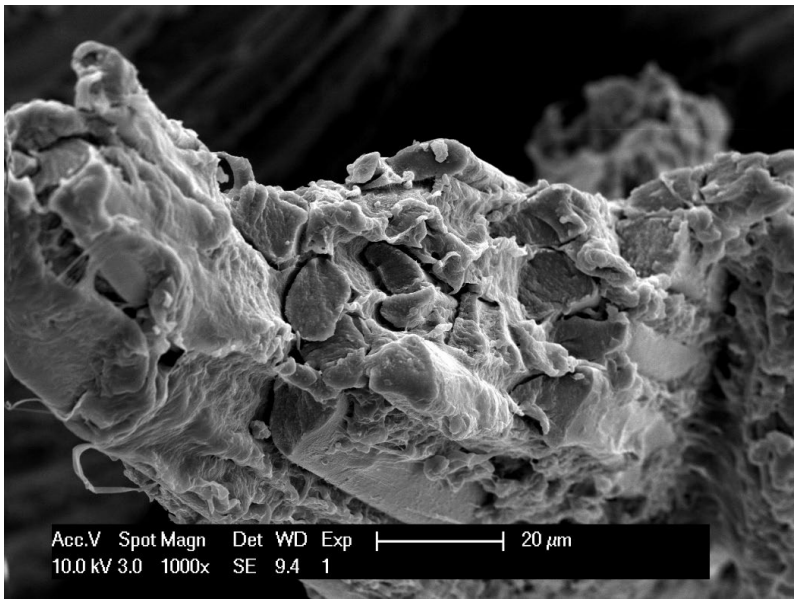

Figure 3. SEM image showing the impregnation quality with the matrix penetrating in between the individual fibres

3.2 *Optical investigation of the selected silk fabrics with SEM*

An optical evaluation of the used silk woven fabric architectures is presented in Figure 4. As observed in Figure 4a, the F1 fabric design has a warp/weft balanced character with untwisted fibres in both warp and weft fabric directions. On the other hand, fabrics F2 and F3 show a highly unbalanced character (Figure 4b, 4c), with untwisted fibres in the warp direction and twisted yarns in the weft direction, whilst having different crimp levels between the two fabrics.

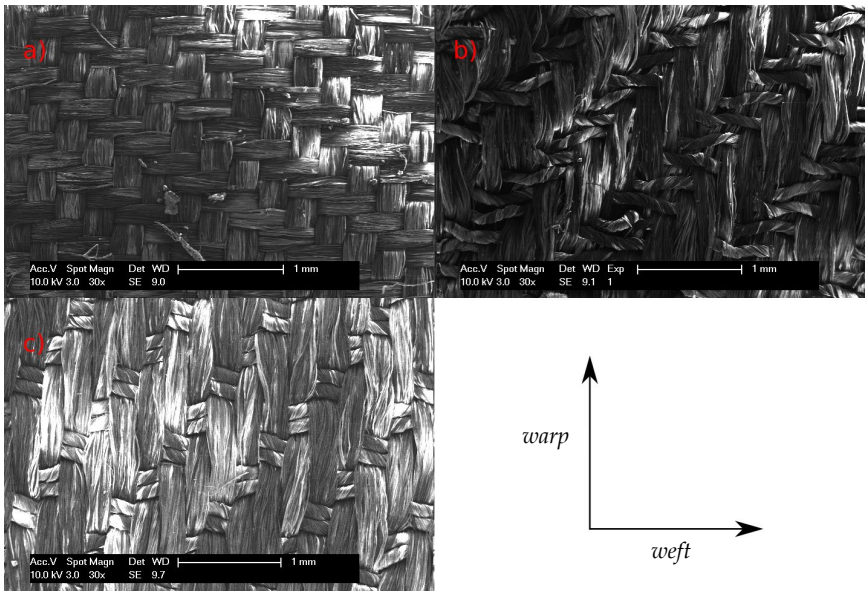

Figure 4. SEM visual inspection of the balanced/unbalanced characteristics of the silk fabrics (a) F1, (b) F2 and (c) F3

3.3 *Mechanical properties*

Tensile properties

The tensile stress-strain representative behaviour of the composites is shown in Figure 5. It is observed that although the F1 fabric is warp/weft balanced in terms of fibre volume, the weft direction shows somewhat higher strength.

On the other hand, the F2 and F3 fabrics show highly different behaviour in warp and weft direction with their weft directions having significantly higher elongation to failure but at the same time lower strength and stiffness. This can be explained by the twisted weft

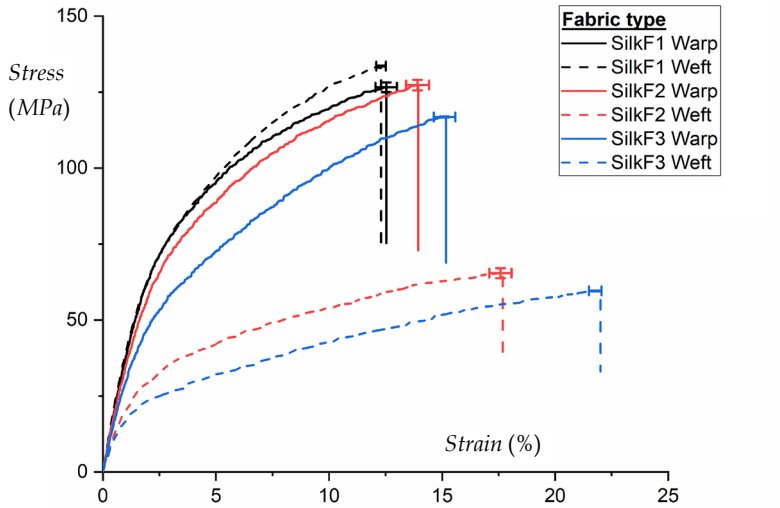

Figure 5. Representative tensile stress-strain curves of the used fabrics once consolidated into composite, tested in warp and weft directions

yarns, which can uncoil during deformation. Furthermore, fabric F3 with the highest anisotropy ratio, shows the highest elong *Strain* (%) h direction when compared, respectively, to the warp and weft directions of the F1 and F2 fabrics. The listed tensile properties in Figure 6 show that, based on the different fabric architectures, a different balance of properties is achieved. It is noted that even though some material configuration shows an increase in strain at failure, the loss of strength and stiffness results in a lower overall toughness, e.g., fabric F3 in weft direction. Therefore, the architecture of the fabric leads to a different balance of tensile properties.

Flexural properties

The representative flexural stress-strain response is presented in Figure 7, where a dependency of the behaviour on fabric architecture and orientation is observed. No direct failure is detected visually, or by a large sudden load drop during testing, thus the flexural tests were manually stopped at 5.5 % strain after confirming that all tested specimens reached a maximum stress, followed by a gradual decreasing trend. Consequently, the strain at failure is considered as the stain at the ultimate flexural stress. This behaviour is believed to be a result of the region under compression dominating the failure, which will be clearly shown and further discussed in section 3.4, using XCT imaging.

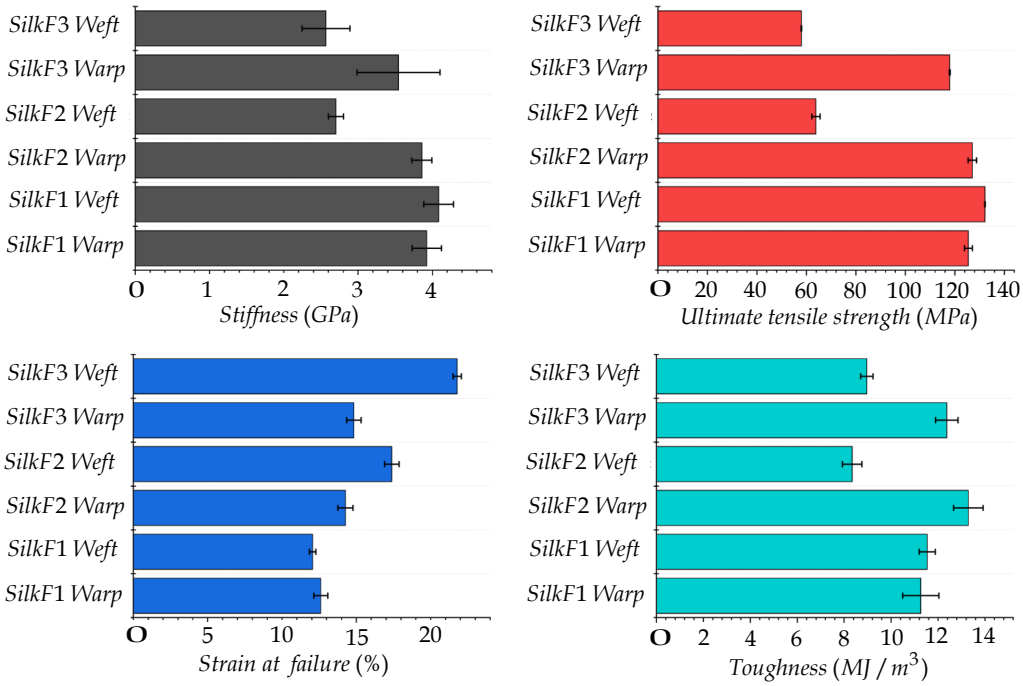

Figure 6. Composite tensile properties as function for of fabric architecture and direction. The toughness is calculated using the total area under the stress-strain curve.

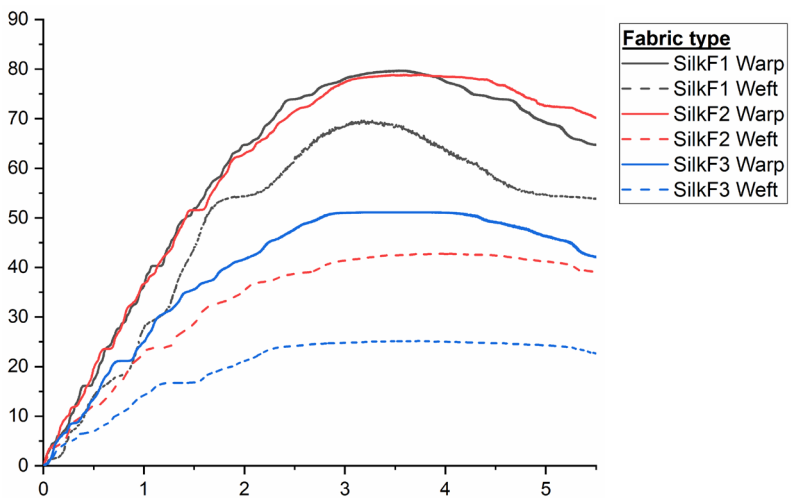

Figure 7. Representative composite flexural stress-strain curves of the used fabrics tested in warp and weft directions

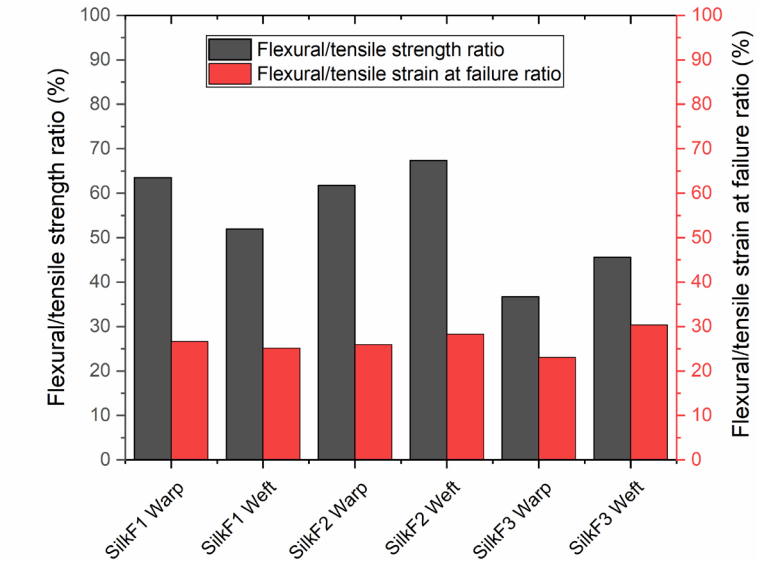

Figure 8. Flexural to tensile strength and strain to failure ratio

It is observed that the twisted yarns in the F2-weft and F3-weft direction have significantly lower stress uptake compared to the straight yarns, as well as the level of crimp has an even stronger influence on the behaviour than in tension. Furthermore, when comparing the flexural to the tensile strength and strain at failure in Figure 8, a clear degradation in properties is observed due to the dominating compressive failure with the flexural to tensile strength ratio staying below 70%, and the strain at failure ratio not surpassing the 30% levels. The latter means that in practice, most of the ductility and thus toughness of the silk fibre composites is lost in case of bending.

*3.4 **2D and 3D imaging: damage characterization***

The acquired XCT volumes provided insight into the structure and the manufacturing defects prior to testing, as presented in Figure 9. Figure 10 shows the same specimen after tensile testing up to failure. One interesting feature observed is that even away from the main failure location that led to catastrophic breakage of the specimen, damage can still be observed in the form of cracks (Figure 10c-e). This behaviour could explain the outstanding toughness of silk fibre composites (in tension) due to damage spreading throughout the volume because of their high ductility, thus allowing to absorb large amounts of energy before failure.

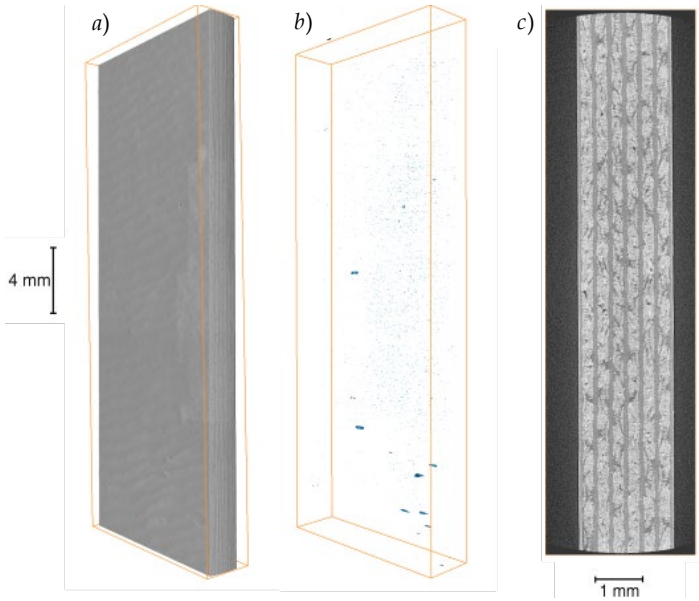

Figure 9. XCT quality control before tensile testing; a) 3D volume of the as produced sample, b) internal manufacturing defects and c) grayscale 2D image of the cross-section

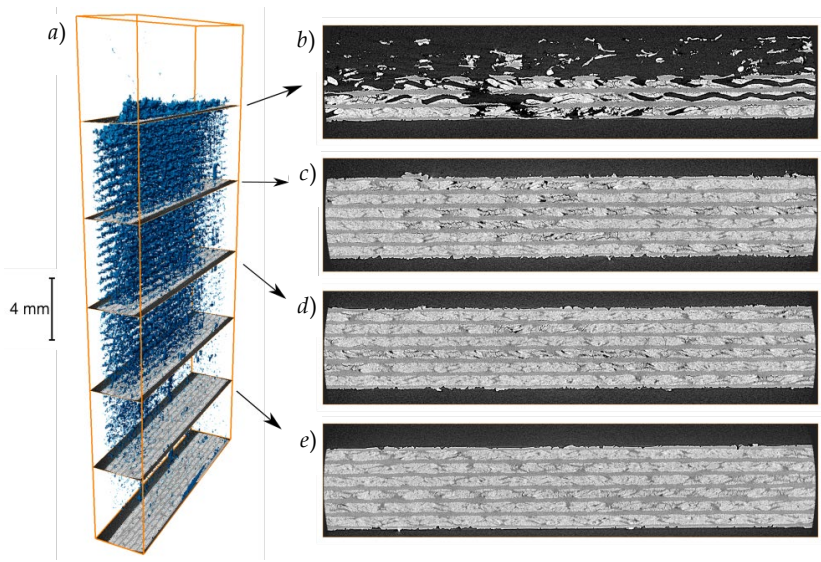

Figure 10. XCT imaging of silk fibre composite (F1 fabric) after tensile testing up to failure; a) 3D representation of the internal damage, b) grayscale 2D image at the fractured region, c) ~6 mm away from the failure region, d) ~12 mm away from the failure region and e) ~24 mm away from the failed region.

XCT imaging applied on the composites after flexural testing is shown in Figure 11. The damage is formed mainly on the side of the composite that is subjected to compression, while the region under tension shows little damage formation. Thus, it is concluded and proven that the compressive region is dominating the failure and thus explaining the limited flexural properties compared to the tensile properties.

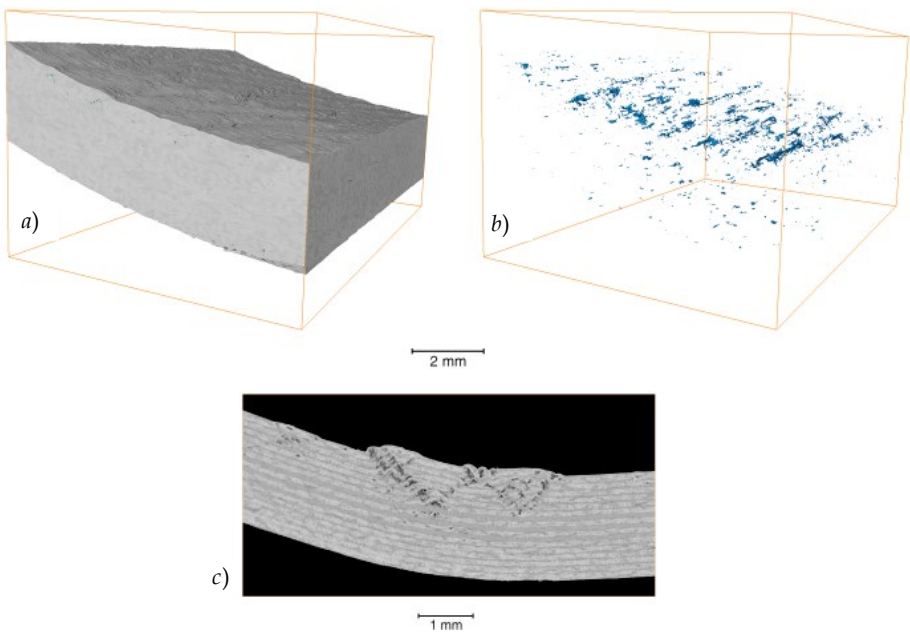

Figure 11. XCT imaging after 3-point bending testing; a) 3D volume visualization of silk composites using the F2 fabric and b) its internal damage after failure, and c) grayscale 2D image of F1 fabric composite showing the concentration of the damage at the compressive region due to the observed characteristic kink-band

SEM imaging, in Figure 12, is performed on the failed regions after tensile testing for the highly warp/weft balanced F1 fabric and the highly unbalanced F3 fabric. All tested specimens showed largely debonded and pulled-out fibres which contributes to the high measured toughness. The balanced fabric F1 shows similar behaviour as expected in both warp and weft directions. On the other hand, the twisted yarns of the unbalanced fabric F3 appear to have shorter debonded fibre length. Therefore, although the strain to failure is higher, possibly due to the unravelling of the twisted yarns, the toughness is still lower as a consequence of this less extensive fibre debonding area. The latter is a failure mechanism with a strong contribution to the toughness of composites [37–39].

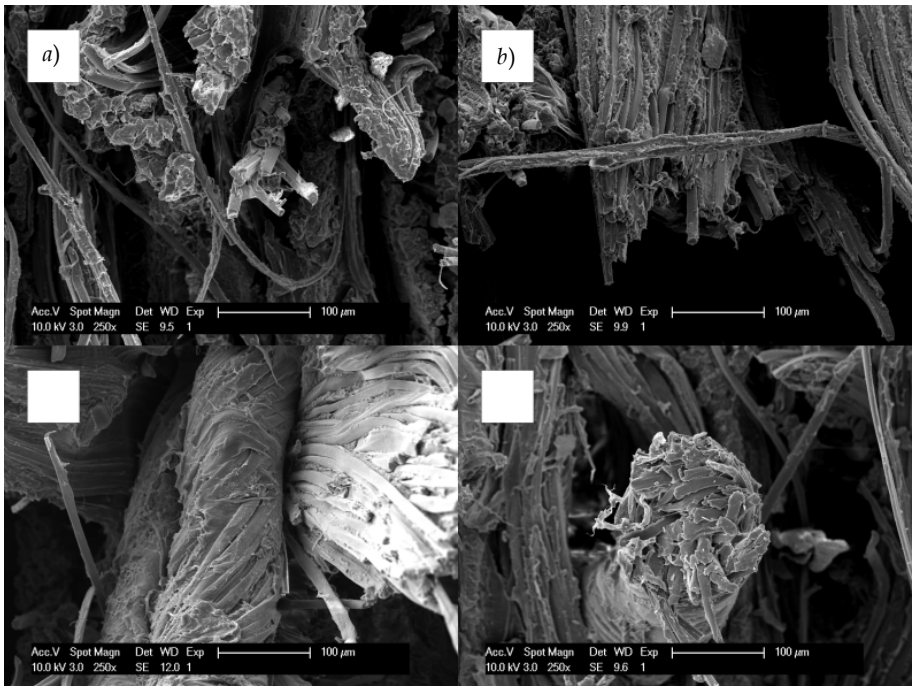

Figure 12. SEM tensile fractured surfaces of silk composites of a) F1 fabric tested in warp and b) weft directions followed by the unbalanced c) F3 tested in warp and d) weft directions

In Figure 13 the tensile failure of silk fibres at high magnifications is presented, showing the deformation at the fractured surface of fibre. It appears that directly near the fractured region the fibres experience some yielding resulting to formation of necking. This damage formation is typically observed in ductile fibres, such as steel fibres (Table 1), and further explains the high energy needed to result into failure of silk fibre composites.

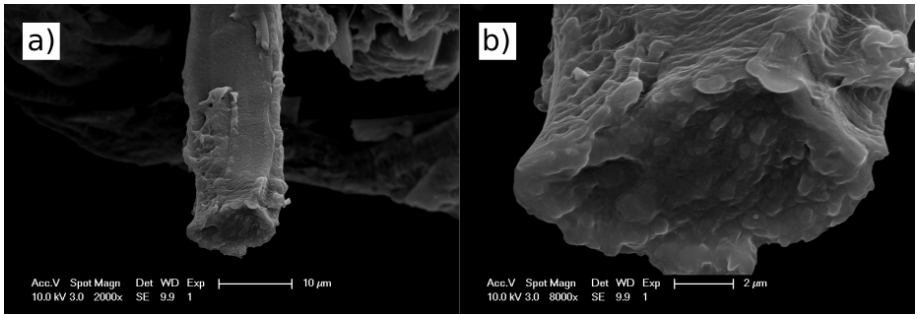

Figure 13. SEM tensile failure of silk fibre at a) ×2000 and b) ×8000 magnification

4 Conclusions

This research investigates the mechanical properties (tensile and flexural) of silk fibre composites, and includes three fabrics with different architectures, produced with a thermoplastic matrix with high ductility. The choice of the polymer matrix was based on allowing the silk fibres to reach their outstanding ductility. The tensile results showed that the silk composites achieve high strain at failure (more than 20%) and toughness (up to 13 MJ/m^3). Furthermore, the architecture of the fabric may result in a trade-off of strength and strain to failure. This is something that should be considered or possibly exploited in designing with silk fabrics for certain applications. XCT 3D imaging of the internal volume revealed that cracks are formed throughout the gauge length of the material and not only in the finally failed region. In addition, SEM imaging on the failed surfaces showed largely debonded fibres and fibre pull-out. All of the above mentioned mechanisms contribute to the total energy absorption, explaining the high toughness of silk fibre composites compared to other natural (plant) or synthetic fibre composites. The measured flexural properties are significantly lower than their tensile counterparts. Particularly the strain at failure in bending reached only 25%-30% of the tensile strain at failure, which essentially limits the intrinsic ductility of the fibres in bending-dominated loading applications. XCT highlighted that the failure is dominated by fibre kinking at the compressive side of the bending specimens and could explain the degradation in flexural properties. The toughness of silk fibre composites requires a ductile matrix to fully enable the energy absorption mechanisms in tension. These ductile matrices are often accompanied by low stiffness, which results in weakened support of the fibres in bending, and thus limited performance in this loading configuration. The research demonstrates the importance of the selection of the matrix for these fibres, in function of the intended applications.

CRediT authorship contribution statement

Alexandros Prapavesis: Conceptualization, Methodology, Data curation, Writing - Original Draft, Formal Analysis, Investigation, Visualization. **Penelope Kopana**: Data curation, Formal analysis, Writing – review & editing, Investigation, Visualization. **Weijing Wu**: Methodology, Investigation, Writing – review & editing. **Jeroen Soete**: Methodology, Visualization, Writing – review & editing. **Yasmine Mosleh**: Conceptualization, Writing - Review & Editing, Supervision. **Aart Willem van Vuure**: Conceptualization, Writing - Review & Editing, Funding Acquisition, Supervision.

Acknowledgements

The author A. Prapavesis is sincerely grateful for the financial support of The Interreg North-West Europe Smart Circular Bridge project under the grant agreement No NEW 993. Furthermore, the authors would like to acknowledge the KU Leuven project C24/17/052, the FWO large infrastructure I013518N project and the KU Leuven XCT core faculty (https://xct.kuleuven.be/) regarding the XCT characterization of composites.

Declaration of competing interest

The authors declare that they have no competing financial interests or personal relationships that could have appeared to influence this work.

References

[1] Pickering KL, Efendy MGA, Le TM. A review of recent developments in natural fibre composites and their mechanical performance. *Compos Part A Appl Sci Manuf* 2016;83:98–112. https://doi.org/10.1016/j.compositesa.2015.08.038.

[2] Joshi S V., Drzal LT, Mohanty AK, Arora S. Are natural fiber composites environmentally superior to glass fiber reinforced composites? *Compos Part A Appl Sci Manuf* 2004;35:371–6. https://doi.org/10.1016/j.compositesa.2003.09.016.

[3] Symington MC, Banks WM, West OD, Pethrick RA. Tensile testing of cellulose based natural fibers for structural composite applications. *J Compos Mater* 2009;43:1083–108. https://doi.org/10.1177/0021998308097740.

[4] Dittenber DB, Gangarao HVS. Critical review of recent publications on use of natural composites in infrastructure. *Compos Part A Appl Sci Manuf* 2012;43:1419–29. https://doi.org/10.1016/j.compositesa.2011.11.019.

[5] Bensadoun F, Verpoest I, Baets J, Müssig J, Graupner N, Davies P, et al. Impregnated fibre bundle test for natural fibres used in composites. *J Reinf Plast Compos* 2017. https://doi.org/10.1177/0731684417695461.

[6] Bensadoun F, Depuydt D, Baets J, Verpoest I, van Vuure AW. Low velocity impact properties of flax composites. *Compos Struct* 2017;176:933–44. https://doi.org/10.1016/j.compstruct.2017.05.005.

[7] Javanshour F, Prapavesis A, Pärnänen T, Orell O, Lessa Belone MC, Layek RK, et al. Modulating impact resistance of flax epoxy composites with thermoplastic interfacial toughening. *Compos Part A Appl Sci Manuf* 2021;150:106628. https://doi.org/10.1016/j.compositesa.2021.106628.

[8] Javanshour F, Prapavesis A, Pournoori N, Soares GC, Orell O, Pärnänen T, et al. Impact and fatigue tolerant natural fibre reinforced thermoplastic composites by using non-dry fibres. *Compos Part A Appl Sci Manuf* 2022;161. https://doi.org/10.1016/j.compositesa.2022.107110.

[9] Shao Z, Vollrath F. Surprising strength of silkworm silk. *Nature* 2002;418:741. https://doi.org/10.1038/418741a.

[10] Hardy JG, Römer LM, Scheibel TR. Polymeric materials based on silk proteins. *Polymer* (Guildf) 2008;49:4309–27. https://doi.org/10.1016/j.polymer.2008.08.006.

[11] Shear WA, Palmer JM, Coddington JA, Bonamo PM. A devonian spinneret: early evidence of spiders and silk use. *Science* 1989;246:479–81. https://doi.org/10.1126/science.246.4929.479.

[12] Garwood RJ, Dunlop JA, Knecht BJ, Hegna TA. The phylogeny of fossil whip spiders. *BMC Evol Biol* 2017;17:1–14. https://doi.org/10.1186/s12862-017-0931-1.

[13] Knight DP, Vollrath F. Liquid crystalline spinning of spider silk. *Nature* 2001;410:541–8.

[14] Wise DH. Cannibalism, food limitation, intraspecific competition, and the regulation of spider populations. *Annu Rev Entomol* 2006;51:441–65. https://doi.org/10.1146/annurev.ento.51.110104.150947.

[15] Tang X, Ye X, Wang X, Zhao S, Wu M, Ruan J, et al. High mechanical property silk produced by transgenic silkworms expressing the spidroins PySp1 and ASG1. *Sci Rep* 2021;11:1–9. https://doi.org/10.1038/s41598-021-00029-8.

[16] Zhang X, Xia L, Day BA, Harris TI, Oliveira P, Knittel C, et al. CRISPR/Cas9 Initiated Transgenic Silkworms as a Natural Spinner of Spider Silk. *Biomacromolecules* 2019;20:2252–64. https://doi.org/10.1021/acs.biomac.9b00193.

[17] Mosleh Y, Cajka M, Depreitere B, Ivens J, Sloten J Vander. Smart material and design solutions for protective headgears in linear and oblique impacts: column/matrix composite liner to mitigate rotational accelerations. *Smart Mater Struct* 2023;32. https://doi.org/10.1088/1361-665X/aca575.

[18] Yang K, Guan J, Numata K, Wu C, Wu S, Shao Z, et al. Integrating tough Antheraea pernyi silk and strong carbon fibres for impact-critical structural composites. *Nat Commun* 2019;10:1–12. https://doi.org/10.1038/s41467-019-11520-2.

[19] Gosline JM, Guerette PA, Ortlepp CS, Savage KN. The mechanical design of spider silks: From fibroin sequence to mechanical function. *J Exp Biol* 1999;202:3295–303. https://doi.org/10.1242/jeb.202.23.3295.

[20] Heim M, Keerl D, Scheibel T. Spider silk: From soluble protein to extraordinary fiber. *Angew Chemie* - Int Ed 2009;48:3584–96. https://doi.org/10.1002/anie.200803341.

[21] Pérez-Rigueiro J, Viney C, Llorca J, Elices M. Mechanical properties of single-brin silkworm silk. *J Appl Polym Sci* 2000;75:Pages 1270-1277. https://doi.org/https://doi.org/10.1002/(SICI)1097-4628(20000307)75:10<1270::AID-APP8>3.0.CO;2-C.

[22] Pérez-Rigueiro J, Elices M, Llorca J, Viney C. Tensile properties of silkworm silk obtained by forced silking. *J Appl Polym Sci* 2001;82:1928–35. https://doi.org/https://doi.org/10.1002/app.2038.

[23] Hudson SD, Zhurov V, Grbić V, Grbić M, Hutter JL. Measurement of the elastic modulus of spider mite silk fibers using atomic force microscopy. *J Appl Phys* 2013;113:154307. https://doi.org/10.1063/1.4800865.

[24] Cunniff PM, Fossey SA, Auerbach MA, Song JW, Kaplan DL, Adams WW, et al. Mechanical and thermal properties of dragline silk from the spider Nephila clavipes. *Polym Adv Technol* 1994;5:401–10. https://doi.org/10.1002/pat.1994.220050801.

[25] Osaki S, Ishikawa R. Determination of elastic modulus of spider's silks. *Polym J* 2002;34:25–9. https://doi.org/10.1295/polymj.34.25.

[26] Mosleh Y, Clemens D, Gorbatikh L, Verpoest I, Van Vuure AW. Penetration impact resistance of novel tough steel fibre-reinforced polymer composites. *J Reinf Plast* Compos 2015;34:624–35. https://doi.org/10.1177/0731684415574538.

[27] Van Vuure AW, Vanderbeke J, Mosleh Y, Verpoest I, El-Asmar N. Ductile woven silk fibre thermoplastic composites with quasi-isotropic strength. *Compos Part A Appl Sci* Manuf 2021;147:106442. https://doi.org/10.1016/j.compositesa.2021.106442.

[28] Shah DU, Porter D, Vollrath F. Can silk become an effective reinforcing fibre? A property comparison with flax and glass reinforced composites. *Compos Sci Technol* 2014;101:173–83. https://doi.org/10.1016/j.compscitech.2014.07.015.

[29] Yang K, Ritchie RO, Gu Y, Wu SJ, Guan J. High volume-fraction silk fabric reinforcements can improve the key mechanical properties of epoxy resin composites. *Mater Des* 2016;108:470–8. https://doi.org/10.1016/j.matdes.2016.06.128.

[30] Hamidi YK, Yalcinkaya MA, Guloglu GE, Pishvar M, Amirkhosravi M, Altan MC. Manufacturing silk/epoxy composite laminates: Challenges and opportunities. *AIP Conf Proc* 2019;2065. https://doi.org/10.1063/1.5088283.

[31] Wen J, Zeng Y, Wu C, Guan J, Guo H. Silk Lattice Structures from Unidirectional Silk Fiber–Reinforced Composites for Breaking Energy Absorption. *Adv Eng Mater* 2020;22. https://doi.org/10.1002/adem.201900921.

[32] Bergan AC, Herráez M, González C, Lopes CS. A constitutive model for fiber kinking: Formulation, finite element implementation, and verification. *Compos Part A Appl Sci Manuf* 2020;129. https://doi.org/10.1016/j.compositesa.2019.105682.

[33] Van Vuure AW, Mosleh Y, Vanderbeke J, Verpoest I. Highly Impact-Resistant Silk Fiber Thermoplastic Composites. *Adv Eng Mater* 2023;n/a:2300080. https://doi.org/https://doi.org/10.1002/adem.202300080.

[34] Shubhra QTH, Alam AKMM. Effect of gamma radiation on the mechanical properties of natural silk fiber and synthetic E-glass fiber reinforced polypropylene composites: A comparative study. *Radiat Phys Chem* 2011;80:1228–32. https://doi.org/10.1016/j.radphyschem.2011.04.010.

[35] Yuan Q, Yao J, Chen X, Huang L, Shao Z. The preparation of high performance silk fiber/fibroin composite. *Polymer* (Guildf) 2010;51:4843–9. https://doi.org/10.1016/j.polymer.2010.08.042.

[36] Ho MP, Lau KT, Wang H, Bhattacharyya D. Characteristics of a silk fibre reinforced biodegradable plastic. *Compos Part B Eng* 2011;42:117–22. https://doi.org/10.1016/j.compositesb.2010.10.007.

[37] Bryan Harris. *Engineering composite materials*. 1999. https://doi.org/10.1049/pbpo110e_ch26.

[38] Jollivet T, Peyrac C, Lefebvre F. Damage of composite materials. *Procedia Eng* 2013;66:746–58. https://doi.org/10.1016/j.proeng.2013.12.128.

[39] Karbhari VM, Rydin RW. Impact characterization of RTM composites-II: damage mechanisms and damage evolution in plain weaves. *J Mater Sci* 1999;34:5641–8. https://doi.org/10.1023/A:1004701604299.

[40] Yang K, Wu Z, Zhou C, Cai S, Wu Z, Tian W, et al. Comparison of toughening mechanisms in natural silk-reinforced composites with three epoxy resin matrices. *Compos Part A Appl Sci Manuf* 2022;154:106760. https://doi.org/10.1016/j.compositesa.2021.106760.

[41] Yang K, Wu S, Guan J, Shao Z, Ritchie RO. Enhancing the Mechanical Toughness of Epoxy-Resin Composites Using Natural Silk Reinforcements. *Sci Rep* 2017;7:1–9. https://doi.org/10.1038/s41598-017-11919-1.

[42] Ude A., Ariffin A., Sopian K, Arifin A, Azhari C. The impact damage response of plain woven natural silk/epoxy laminated composite plates. *Int J Eng Sci Technol* 2010;2:128–40. https://doi.org/10.4314/ijest.v2i5.60131.

[43] Tian W, Yang K, Wu S, Yang J, Luo H, Guan J, et al. Impact of hydration on the mechanical properties and damage mechanisms of natural silk fibre reinforced composites. *Compos Part A Appl Sci Manuf* 2021;147:106458. https://doi.org/10.1016/j.compositesa.2021.106458.

[44] Zhang H, Magoshi J, Becker M, Chen JY, Matsunaga R. Thermal properties of Bombyx mori silk fibers. *J Appl Polym Sci* 2002;86:1817–20. https://doi.org/10.1002/app.11089.

[45] Motta A, Fambri L, Migliaresi C. Regenerated silk fibroin films: Thermal and dynamic mechanical analysis. *Macromol Chem Phys* 2002;203:1658–65. https://doi.org/10.1002/1521-3935(200207)203:10/11<1658::AID-MACP1658>3.0.CO;2-3.